PEBA/Na-X multilayer hybrid membrane for CO_2 separation: Influence of Na-X zeolite layer synthesis condition

M.J. Vaezi[a,b,*] **and H. Bagheri**[c]

a. *Research Center of Nanostructure Material, Sahand University of Technology, Sahand New Town, Tabriz, Postal Code: 5331817634, Iran.*
b. *Faculty of Chemical Engineering, Sahand University of Technology, Tabriz, Iran.*
c. *Chemical Injuries Research Center, Systems Biology and Poisonings Institute, Baqiyatallah University of Medical Sciences, Tehran, Postal Code: 143-59-16-471, Iran.*

Abstract. The effects of synthesis time and the number of synthesis layers were investigated on the synthesis of Na-X zeolite sublayer for fabricating a Polyether Block Amide (PEBA)/Na-X hybrid membrane. The CO_2/N_2 separation was considered as the objective function to obtain an effective Na-X sublayer. Scanning Electron Microscopy (SEM) and Atomic Force Microscopy (AFM) studies of the synthesized sublayers reveal that 6 hour synthesis time and one synthesis layer give an Na-X sublayer (ZSL6-1) with sub-micron thickness ($< 1~\mu m$), and roughness of 13 nm. The N_2 permeation (11900 GPU) shows the low mass transfer resistance through the ZSL6-1 sublayer. The ZSL6-1 sublayer in the hybrid structure of the membrane leads to the high stability of the multilayer structure via the anchoring effect of the polymer. Hydroxyl groups, along with positive and negative charges on the surface of the Na-X sublayer, cause to strong bonding of the polymer layer and prevent its delamination. The surface coverage of the sublayer by polymer has increased the mass transfer resistance just for N_2 and increase the perm-selectivity. These properties, along with the high affinity of the Na-X to the adsorption of CO_2, results in a 56% increase in the perm-selectivity of CO_2/N_2 (~ 70) compared to net PEBA (~ 40–50) and the recently reported hybrid membranes.

© 2024 Sharif University of Technology. All rights reserved.

1. Introduction

CO_2 is a significant gaseous pollutant with high corrosive properties. The natural gas stream is one of the most important items in which this gas causes great damage. In addition, increasing the production of CO_2 by some industries and increasing their concentration in the air, create new needs for the chemical industries to investigate and provide effective methods for the separation of CO_2 [1–3]. In the last two decades, membrane separation technology has developed, and

*. *Corresponding author. Tel.: +98 4133459170;*
    Fax: +98 4133444355
    E-mail address: m_vaezi@sut.ac.ir (M.J. Vaezi)

Table 1. Summary of important studies about the separation of CO_2 by the zeolite membranes.

Zeolite membrane	CO_2 permeance (GPU)	CO_2/N_2 selectivity	CO_2/CH_4 selectivity	Ref.
CHA	101.19	–	21.6	[14]
SAPO-34	119.4	21	100	[15]
SSZ-13	238.8	10	80	[16]
DD3R	767.16	30	269	[17]
ALPO-18	1940.29	45	202	[18]
SSZ-13	2191.04	–	60	[19]
MFI	3731.34	–	4	[20]
CHA	5074.62	–	54	[21]
FAU	564	–	13.6	[22]
FAU	77	9	51	[23]
FAU	100	6	28	[23]
FAU	20	5	18	[23]
FAU	3.9	20	–	[23]
FAU	100	36	–	[23]
FAU	120	22	–	[23]
FAU	10	–	20	[23]
FAU	5970.14	30	–	[24]

the advantages of this technology made it a strong competitor with other technologies [2,4].

One of the promising strategies for improving the separation performance of membranes in the separation of CO_2 is a composite structure of organic-inorganic multilayer hybrid membranes [5,6]. The motivation for fabricating multilayer hybrid membranes is to achieve a high performance membrane at low cost. The formation of a selective layer of multilayer hybrid membrane with a more minor quantity requirement of material has decreased the cost. Therefore, some expensive and high performance materials can be used [7]. Several review papers have reported that PEBA (Polyether Block Amide) polymer as an organic membrane has excellent potential for separating acid gas such as CO_2, and can be used as a selective top layer in multilayer hybrid membranes [6,8–10]. The multilayer hybrid membrane with high selective top layer must have a suitable sublayer. The small pore size, narrow pore size distribution, smooth surface, and low thickness of the sublayer, along with the low mass transfer resistance and good bonding to support and top layer are the essential parameters in deciding to choose a proper sublayer in multilayer hybrid membranes. Due to the high porosity and narrow pore size distribution of zeolites, using a zeolitic layer as a sublayer, eliminates the need to investigate many of the parameters for obtaining the appropriate sublayer [11–13]. In addition, the high adsorption affinity of zeolites for CO_2 can be another

advantage of using zeolites for this target. Table 1 shows the summary of important studies about the separation of CO_2 by the zeolite membranes, which can be used as a sublayer in a multilayer hybrid membranes. Nevertheless, these membranes (except for FAU zeolite membranes) have shown some drawbacks (expensive structure directing agent and low reproducibility of their synthesis), which might be the reasons not to select them as sublayers.

FAU zeolites (Na-X and Na-Y types) have a very high affinity for the adsorption of acid gases in comparison with other zeolites. Therefore, FAU zeolites with low synthesis cost and high reproducibility is a good candidate for our purpose [25,26].

Chen et al. [27] synthesized a hybrid membrane including a zeolite Y inorganic layer, selective PEBA layer, and Poly Dimethyl Siloxane (PDMS) cover layer on top of the Poly Ether Sulfone (PES) as support. The final membrane showed a good perm-selectivity for CO_2/N_2 (30) and CO_2 permeance (940 GPU) at $57°C$ compared to the membrane without the zeolite Y sublayer. However, they have not reported any information about the synthesis conditions of the zeolite layer as an effective sublayer and the effect of important parameters such as synthesis time and the number of synthesis layers. In addition, the effect of these parameters was never investigated till now. Therefore, due to the importance of the synthesis condition of the Na-X zeolite sublayer to obtain the final multilayer

PEBA/Na-X hybrid membrane, the investigation of the synthesis time and the number of synthesis layer effect on the synthesis of Na-X zeolite sublayer with the objective function of maximizing the CO_2 separation performance is vital.

In this work, we considered synthesis time and the number of synthesis layers as an effective parameter on the synthesis of the Na-X zeolite sublayer to obtain an effective Na-X sublayer for fabricating a PEBA/Na-X hybrid membrane for CO_2 separation, which nobody has reviewed yet. The Na-X zeolite sublayer was synthesized via the in-situ hydrothermal approach on the α-alumina support with different designed synthesis conditions. Then, the PEBA layer was coated via a dip-coating technique on the synthesized Na-X zeolite sublayers using a PEBA polymer solution. The morphology and crystallinity of the synthesized zeolite sublayers and the prepared hybrid membranes were characterized by SEM and XRD analyses, respectively. In addition, the Atomic force microscopy (AFM) analysis was used to study the surface roughness of the synthesized zeolite sublayer as an important parameter of a proper sublayer. For studying the ability of the obtained hybrid membranes to separate CO_2, the gas permeation tests of pure N_2 and CO_2 were carried out as a function of feed pressure.

2. Material and methods

2.1. Materials

For the synthesis of Na-X zeolite sublayer, the silicon and aluminum precursors were aluminum foil (Al> 99%, solid state, size: 2.54 cm × 50 m, Merck) and silica sol (Ludox, 30 wt% SiO_2 in H_2O, Milky white color, pH = 9.8, Aldrich), respectively. Sodium hydroxide (NaOH, solid state, Tablet shape, Mw = 40 g/mol, Merck, > 99%) and deionized water (TDS = 0, pH = 5.5, Kasra Co.) were utilized as mineralizing and reaction medium, respectively. PEBA (Grade 1657, approximately 40 wt% Polyamide 6 (PA6) and 60 wt% PEO, 1.14 g/cm³, yellow particles with a spherical shape, purchased from Pars Shimi gostar Co.) was used for the formation of polymer selective layer in multilayer hybrid membranes.

2.2. Preparation and procedures

The hydrothermal method with conventional heating and dip-coating method was employed to prepare multilayer hybrid membranes, including PEBA selective layer and Na-X zeolite layer as the sublayer. Figure 1 shows the procedures for the preparation of multilayer hybrid membranes. The molar ratio of precursor used for synthesizing the zeolite sublayer on the outer surface of the home-made tubular α-alumina support (7 cm length; 10 mm outer diameter; 6 mm inner diameter) was $10SiO_2{:}0.5Al_2O_3{:}35Na_2O{:}1000H_2O$. The

Table 2. The different hydrothermal conditions designed and applied for synthesis of Na-X zeolite sublayers on the outer surface of tubular α-alumina support.

Sample*	Synthesis time (h)	Number of synthesis layer
ZSL24-1	24	1
ZSL12-1	12	1
ZSL6-1	6	1
ZSL6-2	6	2
ZSL12-2	12	2

*Sample code: Zeolite Sub-Layer (ZSL).
Followed by synthesis time (h) and
number of synthesis layer.

precursor was prepared by mixing the appropriate two precursor solutions named aluminate and silicalite. The aluminate solution was prepared by dissolving amounts of deionized water, sodium hydroxide, and pure aluminum foil. In addition, the silicalite solution was made by mixing amounts of deionized water, sodium hydroxide, and silica sol. The two prepared solutions were heated at 60°C for 15 min and then mixed to obtain a uniform clear solution. In order to synthesize a zeolite sublayer on the outer surface of the tubular α-alumina support, two ends of the tubular support were closed by Teflon tape and placed in an autoclave, which was filled with synthesis precursor. The synthesis was carried out at 75°C for specific hours. The synthesized sublayers were washed with deionized water several times, and dried at 110°C for 3 hours.

To find the proper hydrothermal synthesis conditions an effective Na-X sublayer, a precursor molar ratio with the appropriate synthesis temperature were chosen, along with the different synthesis times, and number of synthesis layers. The different applied synthesis times, and number of synthesis layers are presented in Table 2.

After the preparation of the zeolite sublayer, to finalize the fabrication of multilayer hybrid membranes, the PEBA was coated on the surface of the synthesized zeolite sublayer by the dip-coating method. Accordingly, one end of the synthesized zeolite sublayers was closed by Teflon tape. Then, they were immersed vertically in the PEBA solution (5 wt% PEBA solution in ethanol/H_2O (30/70, v/v)) for 30 s at room temperature. The final membrane was dried at room temperature for 24 hours. The coding of the hybrid membranes along with the number of PEBA coating for each one is given in Table 3.

2.3. Morphology and crystallinity

The crystalline structure of the synthesized Na-X sublayers was determined by XRD patterns. XRD analysis was carried out on a Bruker D8 ADVANCE X'Pert diffractometer using CuKa ($l = 1.54$ Å) ra-
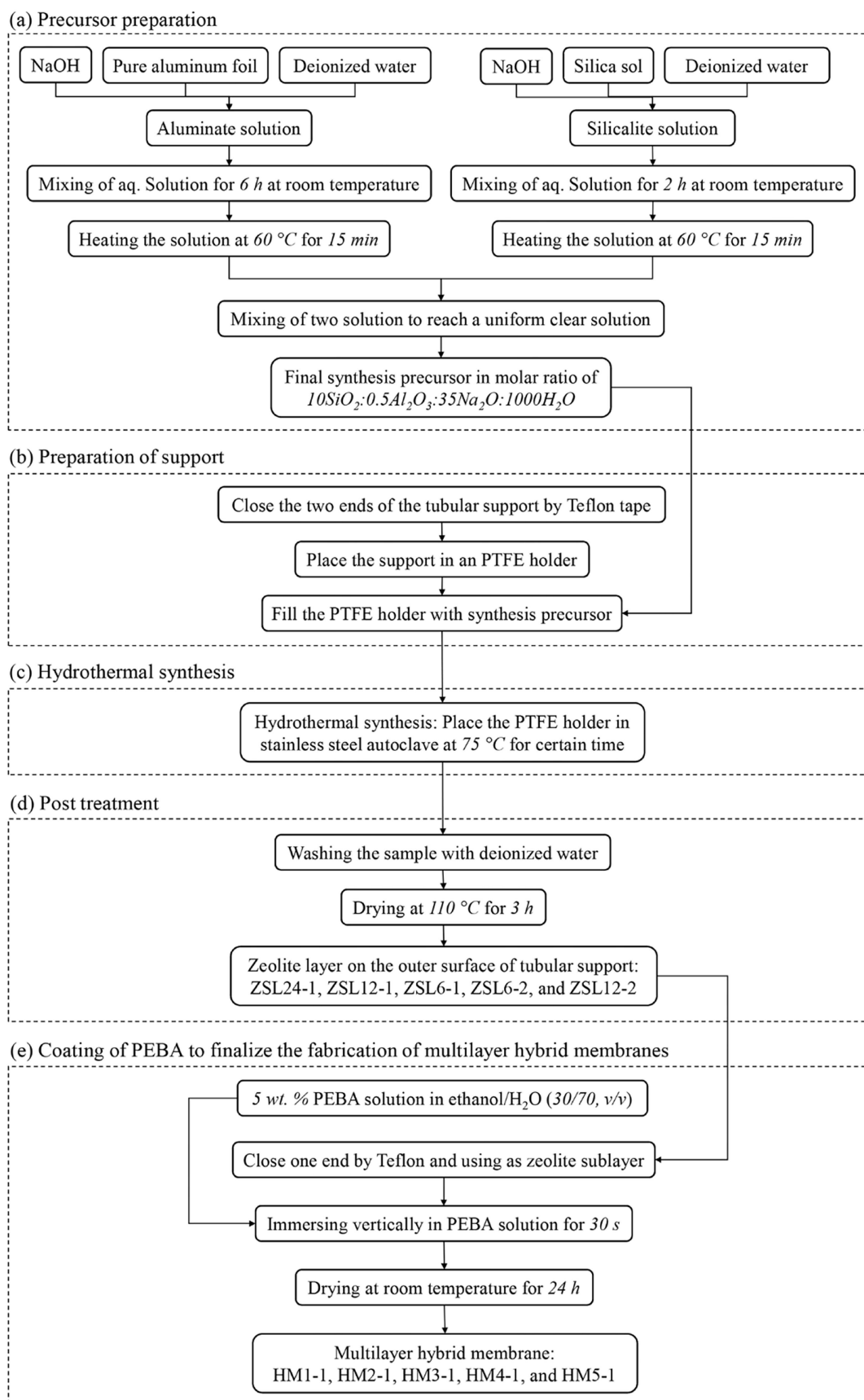
(a) Precursor preparation

| NaOH | Pure aluminum foil | Deionized water |

↓

Aluminate solution

↓

Mixing of aq. Solution for *6 h* at room temperature

↓

Heating the solution at *60 °C* for *15 min*

| NaOH | Silica sol | Deionized water |

↓

Silicalite solution

↓

Mixing of aq. Solution for *2 h* at room temperature

↓

Heating the solution at *60 °C* for *15 min*

↓

Mixing of two solution to reach a uniform clear solution

↓

Final synthesis precursor in molar ratio of
$10SiO_2{:}0.5Al_2O_3{:}35Na_2O{:}1000H_2O$

(b) Preparation of support

Close the two ends of the tubular support by Teflon tape

↓

Place the support in an PTFE holder

↓

Fill the PTFE holder with synthesis precursor

(c) Hydrothermal synthesis

Hydrothermal synthesis: Place the PTFE holder in
stainless steel autoclave at *75 °C* for certain time

(d) Post treatment

Washing the sample with deionized water

↓

Drying at *110 °C* for *3 h*

↓

Zeolite layer on the outer surface of tubular support:
ZSL24-1, ZSL12-1, ZSL6-1, ZSL6-2, and ZSL12-2

(e) Coating of PEBA to finalize the fabrication of multilayer hybrid membranes

5 wt. % PEBA solution in ethanol/H_2O (*30/70, v/v*)

↓

Close one end by Teflon and using as zeolite sublayer

↓

Immersing vertically in PEBA solution for *30 s*

↓

Drying at room temperature for *24 h*

↓

Multilayer hybrid membrane:
HM1-1, HM2-1, HM3-1, HM4-1, and HM5-1

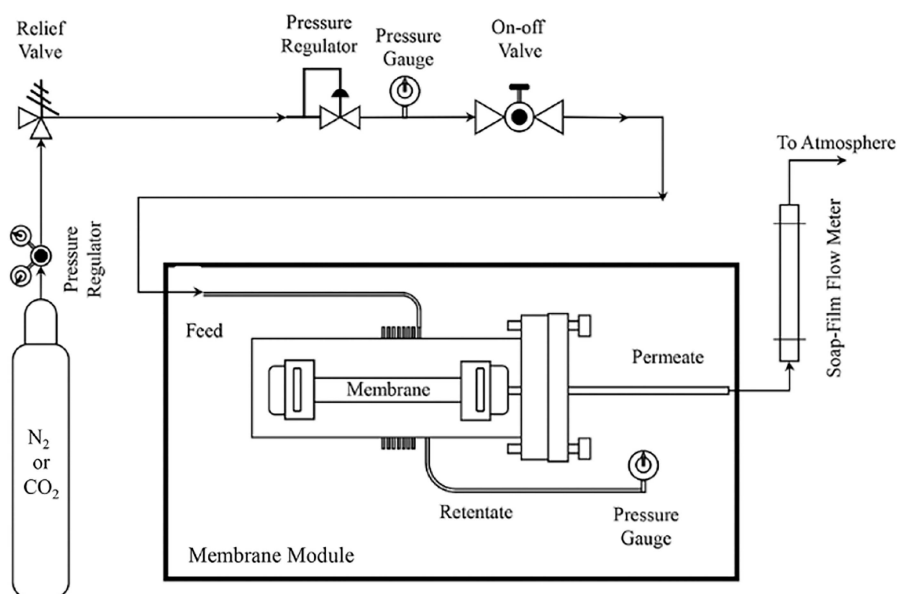**Figure 1.** Procedures for the preparation of multilayer hybrid membranes.

Figure 2. Schematic of laboratory membrane-testing unit.

Table 3. The coding of the hybrid membranes along with the number of PEBA coating for each one.

Sample*	Sublayer	Number of PEBA coating
HM1-1	ZSL24-1	1
HM2-1	ZSL12-1	1
HM3-1	ZSL6-1	1
HM4-1	ZSL6-2	1
HM5-1	ZSL12-2	1
HM2-2	ZSL12-1	2
HM3-2	ZSL6-1	2

*Sample code: Hybrid Membrane (HM).

Followed by No. and number of PEBA coating.

diation operating at 40 kV and 40 mA (Step Size = $0.05[°2Th]$). The surface roughness of the synthesized zeolite sublayers was studied by AFM analysis. The morphology and thickness of the synthesized sublayers and fabricated hybrid membranes were observed by scanning electron microscopy (SEM, VEGA\\, 3 nm, TESCAN, Check and SEM, Cam Scan MV2300, LEO 440I, UK).

2.4. Single gas permeation measurements

Single gas permeation measurements of CO_2 and N_2 were carried out to determine the effectiveness of the applied synthesis methods in the forming zeolite layers on the tubular supports and describe the separation performance of the fabricated multilayer hybrid membranes.

The zeolite layers and the multilayer hybrid membranes were placed inside a stainless steel permeation cell and sealed with O-rings. The pure gas is passed through a relief valve, pressure regulator, and on-off valve, and enters the membrane module as feed. A pressure regulator controls the feed pressure. The single gas permeations were measured using a soap-film flow meter under different feed pressures. The laboratory membrane-testing unit is shown in Figure 2, schematically.

The gas permeation was calculated by Eq. (1) [12]:

$$Gas\ Permeation\ Unit\ (GPU) = 10^6 \times \frac{V}{A \times \Delta P}$$

$$\times \frac{273.15}{T} \times \frac{P}{76}, \tag{1}$$

where V (cc/s) is the flow rate of permeated gas, A (cm^2) is the membrane area, P (cmHg) is the atmospheric pressure, T (K) is the temperature of measurement, and Δp (cmHg) is the pressure difference between the membrane sides. The perm-selectivity was defined as the permeance ratio of two pure gases measured at the same temperature (Eq. (2)) [12]:

$$Perm-selectivity = \frac{GPU_1}{GPU_2}. \tag{2}$$

3. Results and discussion

3.1. XRD, SEM, and AFM of the synthesized zeolite sublayer

Figure 3 depicts the XRD patterns of Na-X sublayers (ZSL24-1, ZSL12-1, ZSL6-1, ZSL6-2, and ZSL12-2) synthesized by the different hydrothermal conditions as mentioned in Table 2. The XRD pattern of the synthesized sublayers is in good agreement with those reported in the reference for the Na-X zeolite XRD pattern [28]. The identification peaks of Na-X zeolite
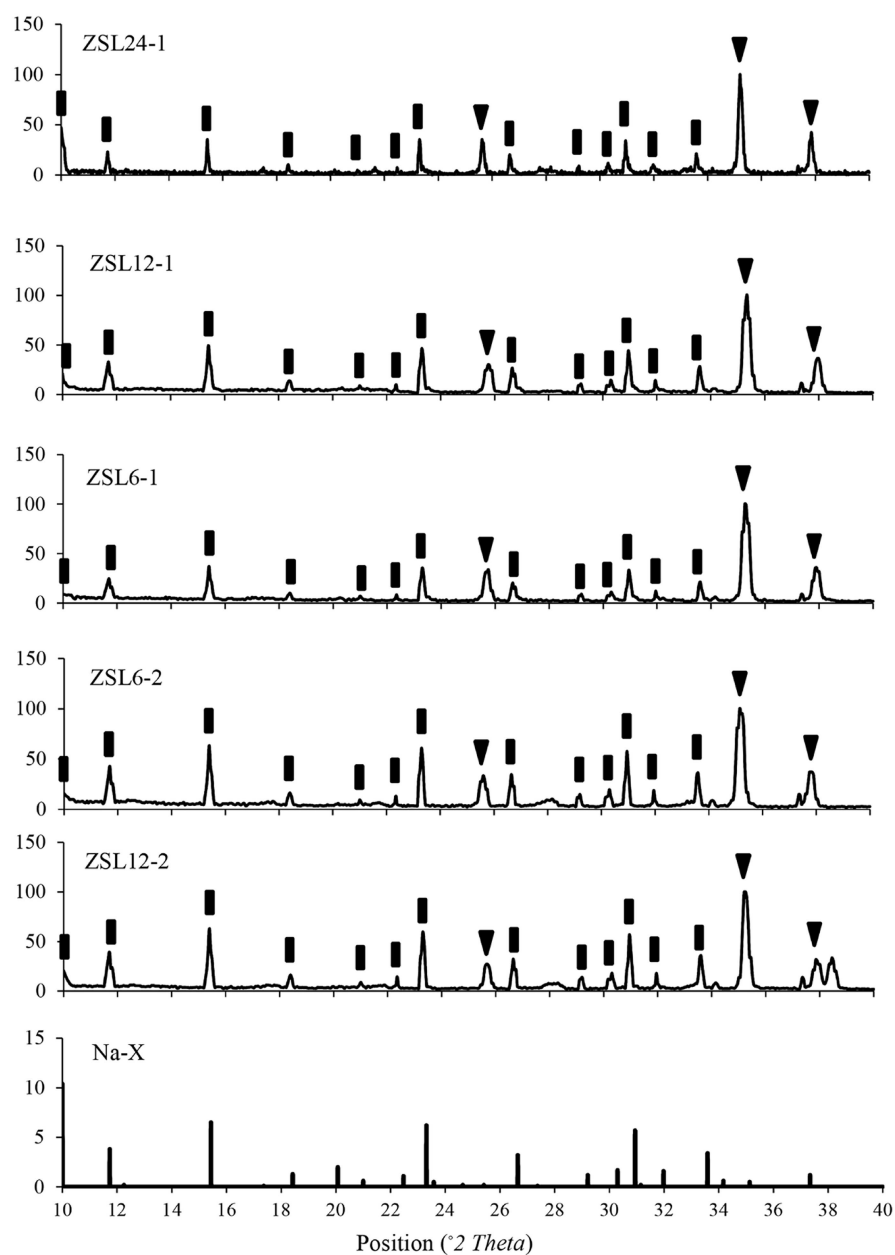
Figure 3. XRD pattern of the synthesized Na-X zeolite (■) sublayers (ZSL24-1, ZSL12-1, ZSL6-1, ZSL6-2, and ZSL12-2) on the α-alumina support (▼).

(2θ = 9.97°, 11.7°, and 15.6°) have appeared in the pattern. Some extra peaks that appeared in the patterns are related to the α-alumina (2θ = 25 − 26°, 34–35°, 37–38°), confirming that the Na-X zeolite sublayers had been synthesized on the outer surface of α-alumina supports. In order to compare the patterns of sublayers, the intensity of the peaks was normalized by the intensity of the highest peak. Comparing the XRD patterns of sublayers reveal that the height of Na-X phase peaks in ZSL6-1 is low compared to others. It can be related to hydrothermal conditions applied to synthesize this zeolite sublayer. The synthesis time of the zeolite layer has a direct effect on the size, and

the crystallinity of the synthesized zeolite crystals. It can also reduce or increase the surface coverage of the support. Increasing the number of synthesis layers is effective on the coverage of the support surface, so that, it can cover the surface parts were not covered by the zeolite crystals in the previous synthesized layers. High surface coverage with large and crystalline zeolite crystals increase the X-ray reflection of the sample and increase the intensity of the related peaks. Therefore, the lower synthesis time with one synthesis layer leads to a low amount and low crystallinity of the synthesized layer (ZSL6-1).
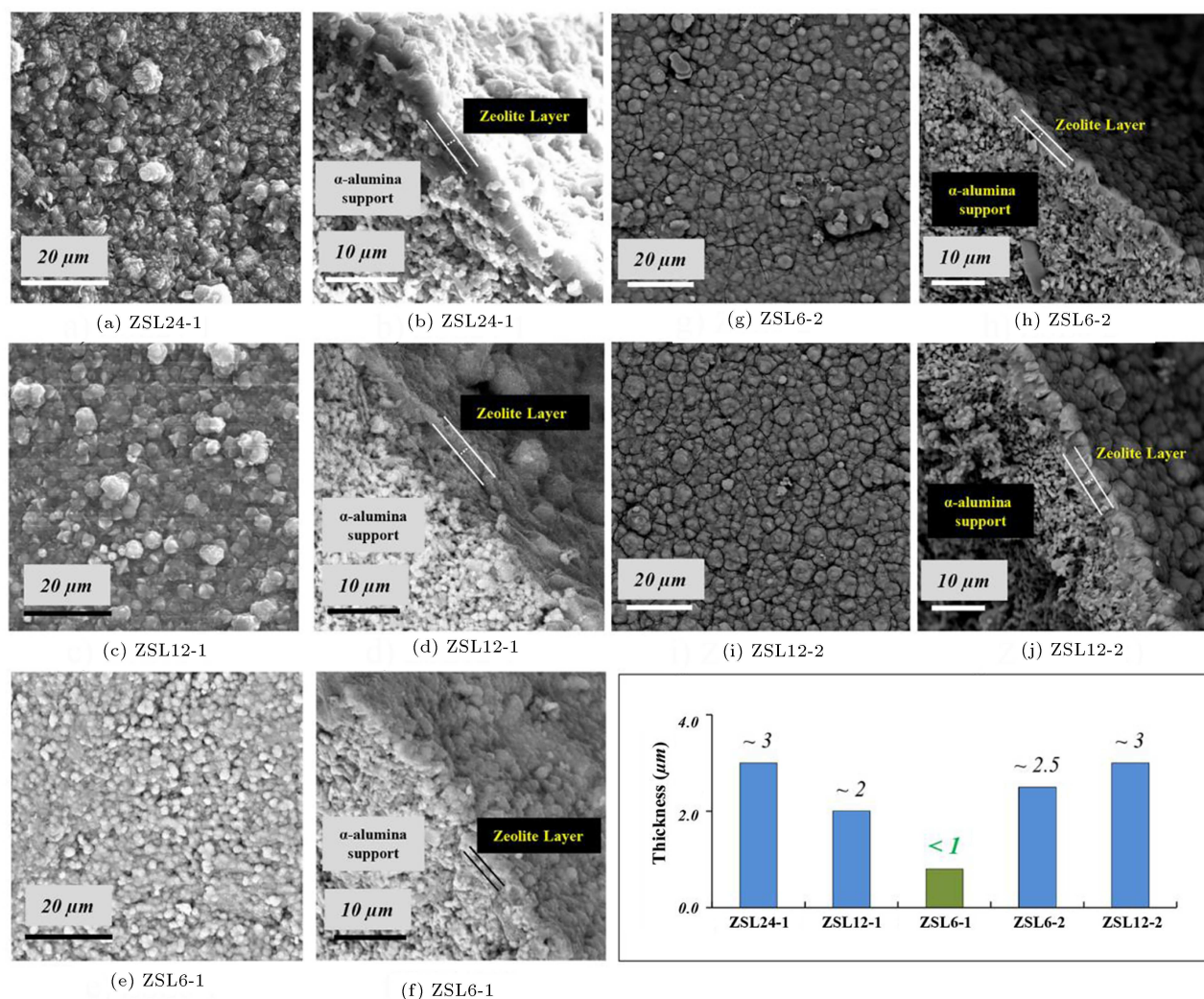
Figure 4 shows the cross-section, and surface

Figure 4. SEM images of the synthesized Na-X zeolite sublayers (ZSL24-1 (a,b), ZSL12-1 (c,d), ZSL6-1 (e,f), ZSL6-2 (g,h), and ZSL12-2 (i,j)) on the α-alumina support.

SEM images of the synthesized Na-X zeolite sublayers (ZSL24-1, ZSL12-1, ZSL6-1, ZSL6-2, and ZSL12-2) on the α-alumina support. The high synthesis time of the zeolite layer leads to the large size of the crystals, and it is possible to improve the surface coverage of the support. The large size of the crystals causes the formation of intercrystalline pores and increases the non-uniformity of the layer. This may occur by the presence of some large-grown zeolite crystals in different parts of the layer. The high synthesis time of ZSL24-1 and ZSL12-1 leads to high thickness, and high coverage of the support surface by zeolite crystals. However, the growth of the large crystals decreases the uniformity of the synthesized zeolite layer. It can affect the quality of the sublayer for the fabrication of the multilayer hybrid membrane.

The low synthesis time of the zeolite layer leads to tiny zeolite crystals and low roughness, but the support surface may be not covered with zeolite crys-tals properly, and the large pores of the support may remain uncovered. However, the surface and cross-section SEM image of ZSL6-1 shows a uniform zeolite sublayer with small zeolite crystals, which grew with better consistency, so there are no large grown crystals on the surface. Therefore, decreasing the synthesis time down to 6 hours is suitable for obtaining a Na-X zeolite sublayer with proper intergrowth and low thickness for fabricating a PEBA/Na-X hybrid membrane.

Increasing the number of synthesis layers can cover the different parts of the support surface that the zeolite crystals did not cover in the previous synthesized layers. It makes possible the filling of the created holes and leads to reduce the roughness of the layer surface. On the other hand, if the previous layers are not suitable, increasing the number of synthesis layers can have a negative effect and cause the growth of large crystals. This increases the thickness of the zeolite layer, causes the non-uniform zeolite layer, and

increases the presence of large intercrystalline pores in the zeolite layer. The zeolite layer with high thickness can crack during the drying step. It increases the possibility of polymer penetration into the zeolite layer and decreases the effective surface area of the final multilayer hybrid membrane.

As can be seen in the SEM images of ZSL6-2 and ZSL12-2 sublayers, by increasing the synthesis layer, the large crystals are decreased on the surface of zeolite sublayers, and the sublayers' thickness becomes more uniform. This is more about the ZSL6-2 synthesized with the ZSL6-1 condition (6 hours in autoclave). On the other hand, by considering the surface images of ZSL6-2 and ZSL12-2, it can be indicated that these sublayers are poorly integrated, and there are many cracks in the synthesized sublayers. This may be due to the thermal shock occurred when the second layer dries at the furnace. Because, by repeating the synthesis, the synthesized sublayer becomes sensitive to a thermal gradient.

Using the calculations related to the images obtained by AFM analysis for the synthesized Na-X zeolite sublayers (ZSL24-1, ZSL12-1, ZSL6-1, ZSL6-2, and ZSL12-2) resulted that the surface roughness is about 36 nm, 24 nm, 13 nm, 27 nm, and 27 nm, respectively (Figure 5). A comparison of the surface roughness of these sublayers with the surface roughness of α-alumina support (200 nm) reveals that the presence of the Na-X zeolite layer on the alumina support reduced the surface roughness. The reduction of the surface roughness can be influenced by the size, and shape of the cavities, and the particles formed on the surface of the zeolite sublayers.

The uniformity of the surface, the small size of the existing crystals, the small pore diameter, and the low crystallinity of the crystals on the surface make the surface smooth. A comparison of the surface roughness of ZSL24-1, ZSL12-1, and ZSL6-1 shows that, decreasing the synthesis time reduces the surface roughness of the zeolite sublayer. Because, the growth of the crystals was decreased, and the support surface pores are covered by zeolite crystals with smooth morphology. These results are in good agreement with
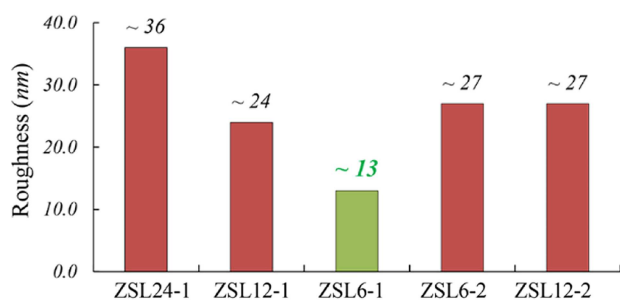
the results of the SEM images. A comparison of the surface roughness of the ZSL6-2 and ZSL6-1 shows that repeating the synthesis of layer leads to more growth of crystals as well as increased crystallinity, and consequently increased roughness. This indicates that the synthesis of the second layer has a significant effect on low times. Comparing the surface roughness of the ZSL12-2 and ZSL12-1 shows that repeating the synthesis of the layer at a high synthesis time does not affect the crystallinity and surface roughness. However, it can increase the layer thickness, which is unsuitable based on the determined target.

3.2. Single gas permeation measurements of the synthesized zeolite sublayer

Figure 6 shows the single gas permeation of N_2 through the synthesized Na-X zeolite sublayers (ZSL24-1, ZSL12-1, ZSL6-1, ZSL6-2, and ZSL12-2) as a function of feed pressure. The single gas permeation of N_2 was carried out to investigate the quality of the synthesized zeolite sublayers, including the coverage amount of the support surface, its efficiency for use as a sublayer, and its mass transfer resistance. Based on the thickness of the zeolite sublayers, the order of permeation should be ZSL6-1> ZSL12-1> ZSL6-2> ZSL12-2 and, or ZSL24-1. However, based on the measurements, the order of permeation is ZSL12-1> ZSL6-1> ZSL6-2> ZSL12-2> ZSL24-1. The ZSL12-1 and ZSL6-1 have approximately the same permeation. The slightly lower permeation of N_2 through the ZSL6-1, despite its lower thickness, can be attributed to its synthesis condition. At low synthesis times (6 hours), the crystals grow smaller and more compact to each other, but in the ZSL12-1 synthesized in 12 hours, the crystals grow more than ZSL6-1, so that the intercrystalline pores are increased and make the sublayer more permeable. The higher permeation through
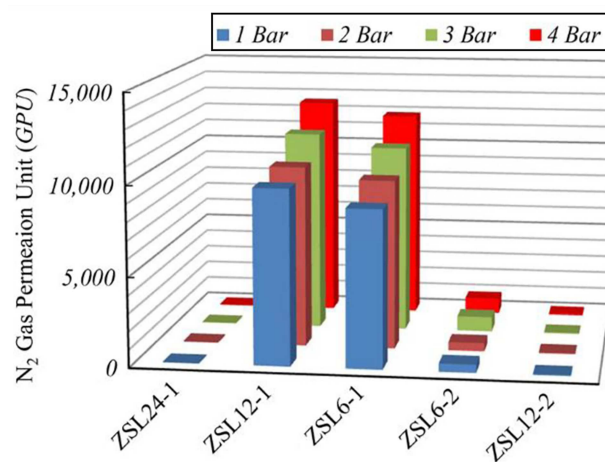
Figure 5. Roughness of the synthesized Na-X zeolite sublayers: ZSL24-1, ZSL12-1, ZSL6-1, ZSL6-2, and ZSL12-2.

Figure 6. Single gas permeation of N_2 through the synthesized Na-X zeolite sublayers (ZSL24-1, ZSL12-1, ZSL6-1, ZSL6-2, and ZSL12-2) as a function of feed pressure.

the ZSL6-2 and ZSL12-2 compared to the ZSL24-1 is related to lower thickness and cracks in the surface of these sublayers. As discussed in the previous sections, by repeating the synthesis, the synthesized sublayer becomes sensitive to a thermal gradient. The thermal shock makes the crack possible in the zeolite layers. The low permeation through ZSL24-1, ZSL6-2, and ZSL12-2 makes the coating of the polymer layer on the surface of these sublayers ineffective.

3.3. SEM of the fabricated multilayer hybrid membranes

Figure 7 shows the SEM images of the HM1-1(a,b), HM2-2(c,d), HM3-2(e,f), HM4-1(g,h), and HM5-1 (i,k). As can be seen in the SEM images of the HM1, HM2, and HM4, the surface morphology of this membrane is similar to that of the surface morphology before the coating of the polymer. In addition, the cross-section images indicate that a very poor polymer layer formed on the surface of these zeolite sublayers,

and no thickness can be considered for them. The created cracks, in addition to the presence of large crystals and a lot of intercrystalline pores in the zeolite sublayers, are the main reason for the very poor polymer layer on their surface. Because, the polymer solution penetrates the zeolite layer and fills the voids between the crystals in the coating step. Also, the presence of hydroxyl groups and different charges on the surface of Na-X zeolite increases the pore penetration of polymer to intercrystalline and non-zeolite pores. Therefore, the polymer layer does not form and fully cover the surface of the zeolite sublayers. This indicates that if an inappropriate surface is used as a sublayer, the poor layer will be obtained even with twice coating the polymer.

The surface SEM image of the HM3-2 shows that the polymer layer completely covers the surface of the membrane, and the surface morphology of this membrane was changed. The cross-section SEM image shows a thin polymer layer on the zeolite sublayer,
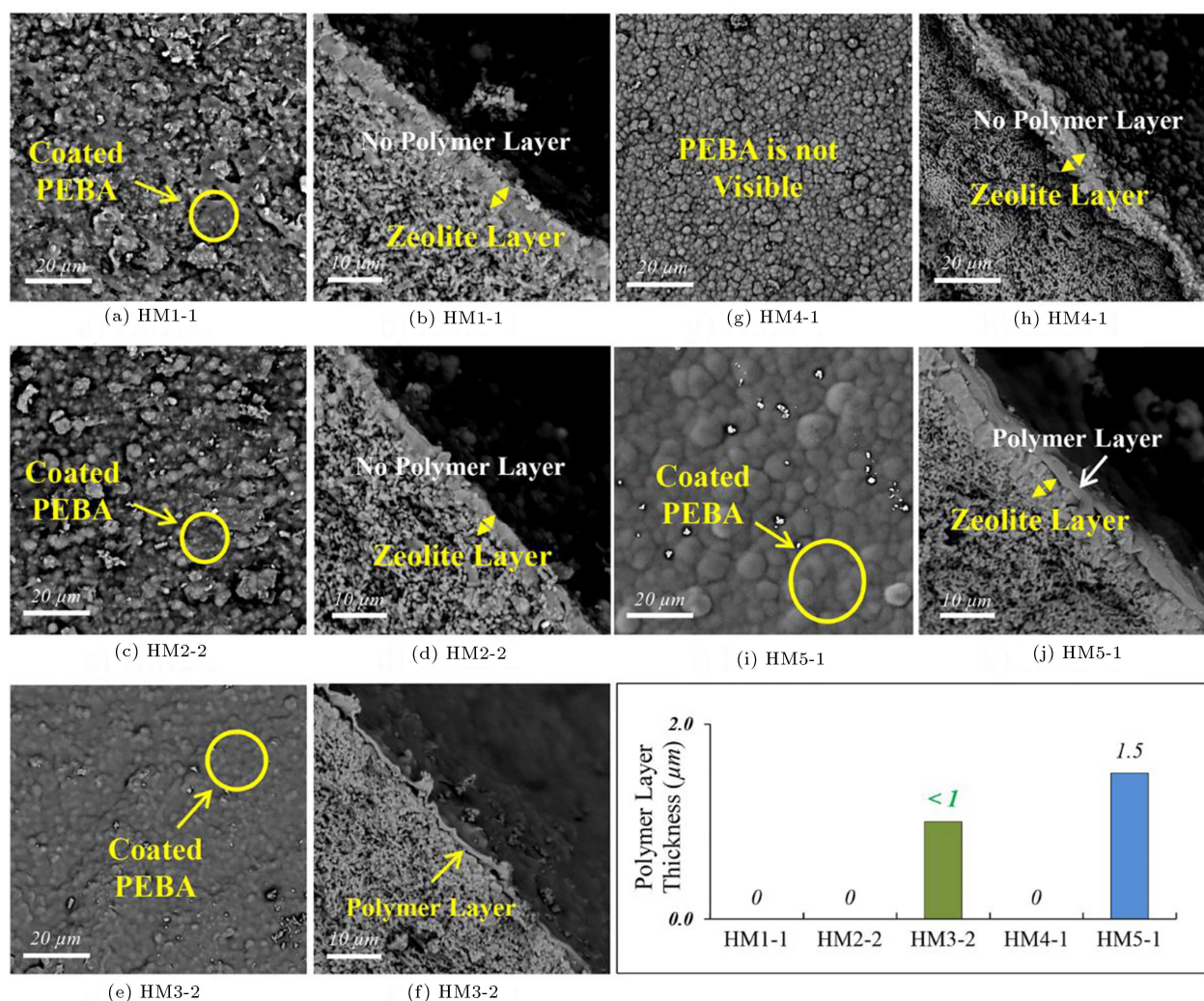

Figure 7. Surface (left) and cross-section (right) SEM images of the HM1-1 (a,b), HM2-2 (c,d), HM3-2 (e,f), HM4-1 (g,h), and HM5-1 (i,j).

with sub-micron thickness. The suitable polymer layer is formed due to the excellent interaction between the zeolite layer and the polymer solution without penetrating the sublayer. This is related to the proper feature (the integrity and smoothness of the surface) of the used zeolite sublayer (ZSL6-1). The SEM images of HM5-1 show that the polymer completely covered the surface of the membrane, and the morphology of HM5-1 has changed over the initial state. According to the cross-section image of the HM5-1, the polymer layer has a thickness of about 1–2 μm. The formation of the polymer layer with micron thickness after the first coating indicates that the polymer has penetrated less into the zeolite layer. The reason is that the non-zeolite pores are located in the outer parts of the zeolite layer, and a small volume of the polymer solution can enter the pores.

3.4. Single gas permeation measurements of the fabricated multilayer hybrid membranes

To measure the permeation of gases accurately (keep the gas permeation amounts in the appropriate range of flow meter accuracy), the feed pressure was selected in a higher range (4–8 Bar). Because, after coating the polymer layer, the permeation of gases through the membranes is reduced. Figure 8 shows the single gas permeation of the CO_2 and N_2, and perm-selectivity of the CO_2/N_2 through the HM1-1, HM2-1, HM3-1, HM4-1, and HM5-1 hybrid membranes as a function of feed pressure. The CO_2 and N_2 permeation is reduced for all hybrid membranes after coating the polymer solution. This is due to the mass transfer resistance made by the polymer solution. However, the gas permeation reduction is different in membranes. The CO_2 and N_2 permeation of HM1-1, HM4-1, and HM5-1 show that the perm-selectivity of CO_2/N_2 is low. The main reasons for the low performance of these membranes are the high thickness of zeolite sublayers, and the presence of intercrystalline pores in zeolite sublayers being filled by the polymer solution. The low perm-selectivity of CO_2/N_2 in HM1-1 ($\sim$1.5) and HM4-1 ($\sim$0.8) reveals the absence of the polymer contribution in the permeation of gases. In these membranes, the polymer solution has filled in some of the non-zeolitic pores and blocked them without forming a polymer layer on the sublayer. Therefore, the gas molecules permeate through the non-zeolitic pores, which are not entirely blocked. This is confirmed by comparing the perm-selectivity of HM1-1 and HM4-1 membranes with the Knudsen selectivity of CO_2/N_2 ($\sim$1.25). The Knudsen selectivity is pressure independent and is proportional to the inverse square root of the molecular weight. The perm-selectivity close to the Knudsen selectivity indicates the presence of non-zeolitic pores with large sizes in the zeolite
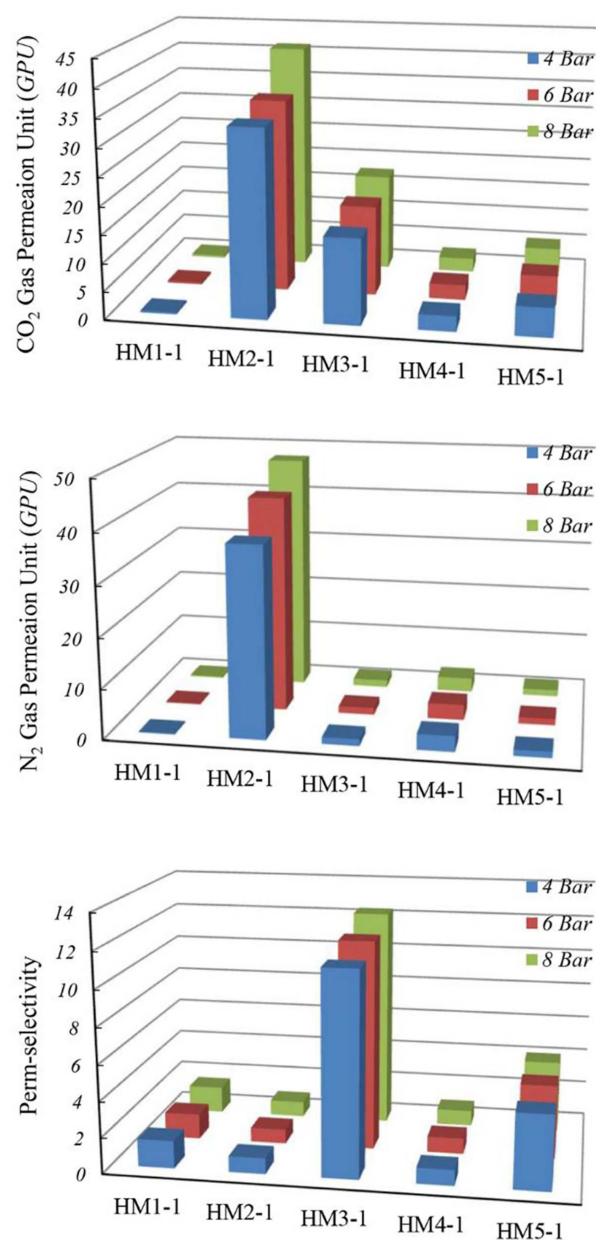

Figure 8. Single gas permeation of the CO_2 and N_2, and perm-selectivity of the CO_2/N_2 through the HM1-1, HM2-1, HM3-1, HM4-1, and HM5-1 hybrid membranes as a function of feed pressure.

sublayer of these membranes so that their mean size is incomparable to the molecular dimensions of gases [17]. Comparing the CO_2 and N_2 permeations in the HM5-1 membrane shows that the CO_2 permeation is about four times more than N_2, so the perm-selectivity of CO_2/N_2 is 4. This indicates that the number of non-zeolitic pores in the ZSL12-2 is less than in the ZSL6-2. Therefore, the polymer has less penetration into the sublayer's pores in HM5-1, and the polymer layer is formed on the surface of the sublayer. In this membrane, the penetration of polymer into the sublayer leads to low permeance of CO_2; however, the

formation of the polymer layer leads to perm-selectivity of 4.

Comparing the CO_2 and N_2 permeations of HM2-1 shows that the perm-selectivity of CO_2/N_2 is low (~0.8), but the gas permeation-despite 100 times reduction-is suitable. High gas permeations and low perm-selectivity show the presence of large non-zeolitic pores in the HM2-1 compared to HM1-1, HM4-1, and HM5-1 membranes according to the reasons mentioned above.

As expected from the SEM and AFM results, ZSL6-1 with low thickness, low roughness, and well-integrated surface can play a good role as a sublayer in the fabrication of a hybrid membrane. In this regard, after coating the polymer solution, the CO_2 and N_2 permeations show proper separation performance (suitable permeation of CO_2 ~16 GPU and CO_2/N_2 perm-selectivity ~12) for the HM3-1 membrane. The surface coverage of the ZSL6-1 sublayer by polymer solution has increased the mass transfer resistance just for N_2 molecules so that the permeation reduction of CO_2 is about ten times less than N_2. Because, the gas permeation mechanism through the PEBA layer is the solution-diffusion mechanism, and the solubility of CO_2 in PEBA polymer is so higher than N_2. The dominance of this mechanism in gas permeation through the membrane indicates the proper coating of the polymer layer on it.

Figure 9 shows the single gas permeation of the CO_2 and N_2, and the perm-selectivity of the CO_2/N_2 through the HM2-2, and HM3-2 hybrid membranes as a function of feed pressure. As can be seen, the CO_2 and N_2 permeation were reduced for HM2-2 by coating the second polymer layer; however, the perm-selectivity of CO_2/N_2 is still low. The reason is the unsuitable sublayer of HM2-2, which had discussed in previous sections. The CO_2 and N_2 permeations through the HM3-2 hybrid membrane show that the CO_2 permeation has remained constant, but the N_2 permeation has reduced. Then, the perm-selectivity is increased up to 70. The reduction of N_2 permeation is attributed to increasing the thickness of the polymer layer due to the second coating of polymer solution so that the N_2 molecules could not permeate through the layer with high density.

Figure 10 schematically shows the effects of the Na-X zeolite sublayer on the formation of the PEBA selective layer and its separation performance in the multilayer structure of the hybrid membrane. As shown, the Na-X zeolite layer synthesized via effective synthesis condition has a positive effect. It leads to an increase in the perm-selectivity of CO_2/N_2 from 40–50 for net PEBA membrane [29,30] to 70 for hybrid structure. This is attributed to the high affinity of the Na-X zeolite sublayer to the adsorption of CO_2. Also, the presence of silanol groups along with charges
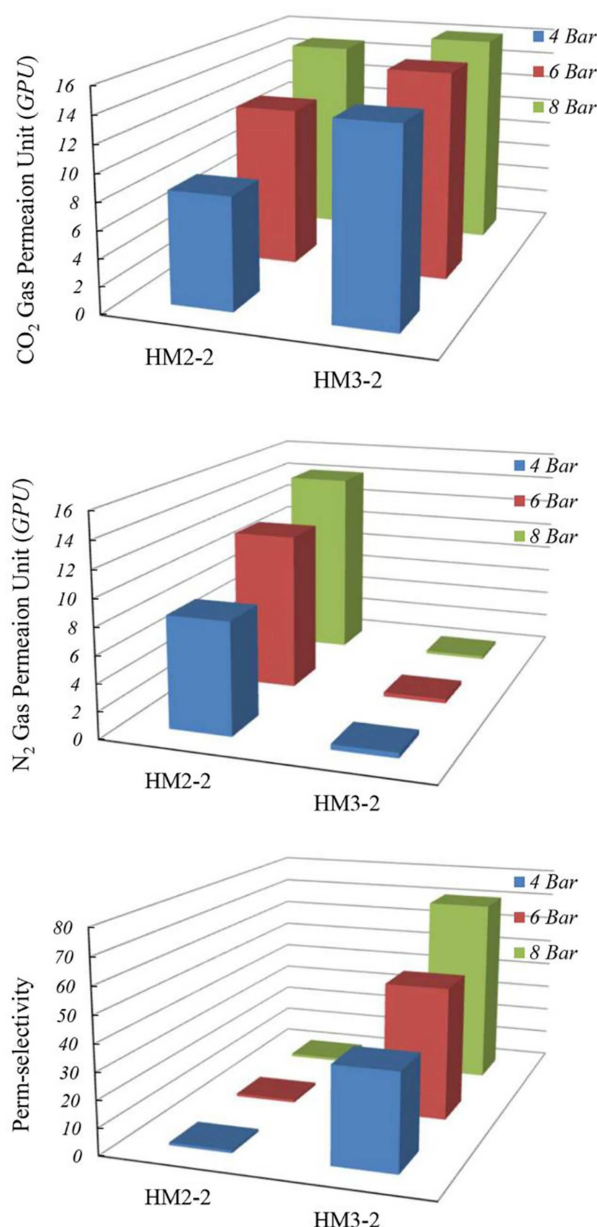

Figure 9. Single gas permeation of the CO_2 and N_2, and perm-selectivity of the CO_2/N_2 through the HM2-2, and HM3-2 hybrid membranes as a function of feed pressure.

on the surface of Na-X zeolite [31,32] could increase the connection of the polymer layer onto the zeolite layer, and prevent the delamination of the polymer layer. So, no delamination of the polymer layer was observed during the experimental steps. On the other hand, the anchoring effect of the polymer and zeolite layer leads to the high stability of the hybrid structure.

3.5. Comparison of the fabricated HM3-2 membrane performance with others

The separation performance of the fabricated membrane (HM3-2) was compared with the other mem-
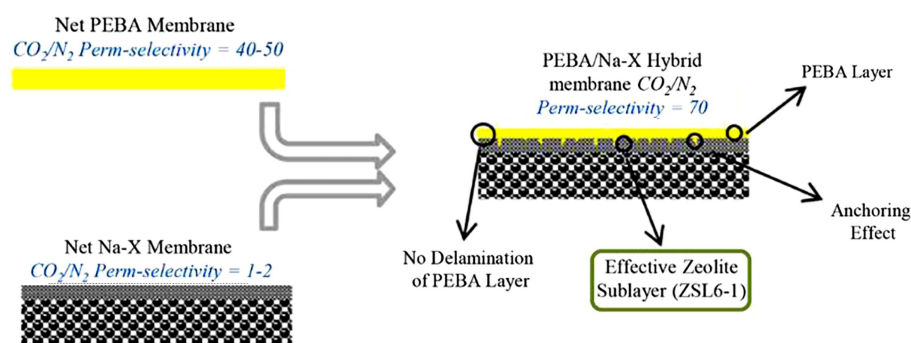
Figure 10. Effect of the Na-X zeolite sublayer on the formation of PEBA selective layer and its separation performance in the multilayer structure of hybrid membrane.

Table 4. Separation performance of HM3-2 membrane in comparison to others.

Support	Sublayer	CO_2/N_2 perm-selectivity	CO_2 permeation (GPU)	Selective layer thickness (μm)	Pressure (Bar)	Ref.
α-alumina	Alumina/Zirconia	Infinite	0.25	140	4	[33]
PSf	Y zeolite	30	940	0.4	1.5 Psig	[27]
PVDF	–	53	21.05	4.2	7	[8]
PSf	PDMS	48	17.28	5	7	[8]
α-alumina	Na-X zeolite	70	16.2	< 1	8	This work

branes in Table 4. The perm-selectivity of the HM3-2 is higher than that of PEBA without and with different sublayers. The CO_2 permeation of HM3-2 is in an acceptable range for being preferable to the recently reported hybrid membranes. So, the presence of the obtained Na-X zeolite sublayer has positively affects the quality and separation performance of the PEBA/Na-X membrane. The simple production method of the HM3-2 membrane makes it preferable over the other membranes. Easy synthesis of the zeolite layer in 6 hours at low temperatures, and polymer coating by the simple coating technique is desired in large-scale production. Also, easier modulating the tubular structure of this type of membrane is a very significant parameter in the industrialization of this technology.

4. Conclusions

Investigating the effects of synthesis time and the number of synthesis layers on the synthesis of Na-X zeolite sublayer with the CO_2/N_2 separation as the objective function showed that increasing the synthesis time and the number of synthesis layer have negative effect for achieving an effective Na-X sublayer. The high synthesis time of the zeolite layer leads to the large size of the crystals. The large size of the crystals causes the formation of intercrystalline pores and increases the non-uniformity of the layer. At coating step, the polymer solution fills in the non-zeolitic pores and block them without forming a polymer layer on the

sublayer. So, low separation performance is achieved. Increasing the number of synthesis layers covers the different parts of the support surface that the zeolite crystals did not cover in the previous synthesized layers. It makes possible the filling of the created holes and leads to reduce the roughness of the layer surface. Also, increasing the number of synthesis layers have a negative effect and cause the growth of large crystals. This increases the thickness of the zeolite layer, causes the non-uniform zeolite layer. The synthesis time of 6 hour and one synthesis layer give an effective Na-X sublayer for fabricating a PEBA/Na-X hybrid membrane with good separation performance compared to other multilayer hybrid membranes in separating CO_2.

Nomenclature

GPU	Gas Permeation Unit
TDS	Total Dissolved Solid
Mw	Molecular weight (g/mol)
wt%	Weight percent
ΔP	Pressure gradient across the membrane (cmHg)
T	Temperature (K)
V	Flow rate of gas permeated through the membrane (cc/s)
A	Membrane area (cm^2)

P Atmospheric pressure (cmHg)

References

1. Khanongnuch, R., Di Capua, F., Lakaniemi, A.M., et al. "Transient-state operation of an anoxic biotrickling filter for H_2S removal", *J. Hazard. Mater.*, **377**, pp. 42–51 (2019).
   DOI: 10.1016/j.jhazmat.2019.05.043

2. Fu, L., Ren, Zh., Si, W., et al. "Research progress on CO_2 capture and utilization technology", *J. CO_2 Util.*, **66**, 102206 (2022).
   DOI: 10.1016/j.jcou.2022.102260

3. Rezakazemi, M., Heydari, I., and Zhang, Zh. "Hybrid systems: Combining membrane and absorption technologies leads to more efficient acid gases (CO_2 and H_2S) removal from natural gas", *J. CO_2 Util.*, **18**, pp. 362–369 (2017).
   DOI: 10.1016/j.jcou.2017.02.006

4. Castro-Muñoz, R., Ahmad, M.Z., Malankowska, M., et al. "A new relevant membrane application: CO_2 direct air capture (DAC)", *Chem. Eng. J.*, **446**(2), 137047 (2022).
   DOI: 10.1016/j.cej.2022.137047

5. Cheng, X., Pan, F., Wang, M., et al. "Hybrid membranes for pervaporation separations", *J. Memb. Sci.*, **541**, pp. 329–346 (2017).
   DOI: 10.1016/j.memsci.2017.07.009

6. Zakariya, Sh., Yeong, Y.F., Jusoh, N., et al. "Performance of multilayer composite hollow membrane in separation of CO_2 from CH_4 in mixed gas conditions", *Polymers*, **14**(7), p. 1480 (2022).
   DOI: 10.3390/polym14071480

7. Dai, Y., Niu, Zh., Luo, W., et al. "A review on the recent advances in composite membranes for CO_2 capture processes", *Sep. Purif. Technol.*, **307**, p. 122752 (2023).
   DOI: 10.1016/j.seppur.2022.122752

8. Momeni, M., Elyasi Kojabad, M., Khanmohammadi, S., et al. "Impact of support on the fabrication of poly (ether-b-amide) composite membrane and economic evaluation for natural gas sweetening", *J. Nat. Gas Sci. Eng.*, **62**, pp. 236–246 (2019).
   DOI: 10.1016/j.jngse.2018.12.014

9. Elyasi Kojabad, M. and Momeni, M. "Fabrication of PEBA polymeric membrane layers on nanostructure PSF supports to separation of CO_2 from N_2 and CH_4", *J. Appl. Chem.*, **15**(54), pp. 101–112 (2020).
   DOI: 10.22075/chem.2020.16150.1546

10. Elyasi Kojabad, M., Babaluo, A.A., Tavakoli, A., et al. "A novel high-performance facilitated transport membrane by simultaneously using semi-mobile and fixed carriers for CO_2/N_2 separation", *Process Saf. Environ. Prot.*, **156**, pp. 304–314 (2021).
    DOI: 10.1016/j.psep.2021.10.017

11. Sadrzadeh, M., Amirilargani, M., Shahidi, K., et al. "Gas permeation through a synthesized composite PDMS/PES membrane", *J. Memb. Sci.*, **342**, pp. 236–250 (2009).
    DOI: 10.1016/j.memsci.2009.06.047

12. Elyasi Kojabad, M., Nouri, M., Babaluo, A.A., et al. "Alumina-PEBA/PSf Multilayer composite membranes for CO_2 separation: experimental and molecular simulation studies", *Sci. Iran.*, **30**(6), pp. 2043–2055 (2022). DOI: 10.24200/sci.2022.57717.5383

13. Afshoun, H.R., Chenar, M.P., Ismail, A.F., et al. "Effect of support layer on gas permeation properties of composite polymeric membranes", *Korean J. Chem. Eng.*, **34**, pp. 3178–3184 (2017).
    DOI: 10.1007/s11814-017-0215-x

14. Maghsoudi, H. and Soltanieh, M. "Simultaneous separation of H_2S and CO_2 from CH_4 by a high silica CHA-type zeolite membrane", *J. Memb. Sci.*, **470**, pp. 159–165 (2014).
    DOI: 10.1016/j.memsci.2014.07.025

15. Li, S., Falconer, J.L., and Noble, R.D. "SAPO-34 membranes for CO_2/CH_4 separations: Effect of Si/Al ratio", *Microporous Mesoporous Mater.*, **110**, pp. 310–317 (2008).
    DOI: 10.1016/j.micromeso.2007.06.016

16. Hong, S., Kim, D., Jeong, Y., et al. "Healing of microdefects in SSZ-13 membranes via filling with dye molecules and its effect on dry and wet CO_2 separations", *Chem. Mater.*, **30**, pp. 3346–3358 (2018).
    DOI: 10.1021/acs.chemmater.8b00757

17. Vaezi, M.J., Babaluo, A.A., and Maghsoudi, H. "Synthesis, modification and gas permeation properties of DD3R zeolite membrane for separation of natural gas impurities (N_2 and CO_2)", *J. Nat. Gas Sci. Eng.*, **52**, pp. 423–431 (2018).
    DOI: 10.1016/j.jngse.2018.01.018

18. Wang, B., Hu, N., Wang, H., et al. "Improved AlPO-18 membranes for light gas separation", *J. Mater. Chem. A*, **3**, pp. 12205–12212 (2015).
    DOI: 10.1039/C5TA01260K

19. Aydani, A., Brunetti, A., Maghsoudi, H., et al. "CO_2 separation from binary mixtures of CH_4, N_2, and H_2 by using SSZ-13 zeolite membrane", *Sep. Purif. Technol.*, **256**, p. 17796 (2021).
    DOI: 10.1016/j.seppur.2020.117796

20. Sandström, L., Sjöberg, L., and Hedlund, J. "Very high flux MFI membrane for CO_2 separation", *J. Memb. Sci.*, **380**, pp. 232–240 (2011). DOI: 10.1016/j.memsci.2011.07.011

21. Kida, K., Maeta, Y., and Yogo, K. "Preparation and gas permeation properties on pure silica CHA-type zeolite membranes", *J. Memb. Sci.*, **522**, pp. 363–370 (2017).
    DOI: 10.1016/j.memsci.2016.09.002

22. Isa, M.A. and Halim, M.H. "Cation-exchanged Na-Y Zeolite: Effect of temperature and ion concentration to membrane performance", *J. Phys. Conf. Ser.*, **1349**, p. 012072 (2019).
    DOI: 10.1088/1742-6596/1349/1/012072

23. Nazir, L.S.M., Yeong, Y.F., and Chew, T.L. "Methods and synthesis parameters affecting the formation of FAU type zeolitemembrane and its separation performance: a review", *J. Asian Ceram. Soc.*, **8**(3), pp. 553–571 (2020).
DOI: 10.1080/21870764.2020.1769816

24. Kusakabe, K., Kuroda, T., Uchino, K., et al. "Gas permeation properties of ion-exchanged faujasite-type zeolite membranes", *AIChE J.*, **45**, pp. 1220–1226 (2004).
DOI: 10.1002/aic.690450608

25. Kumar, S., Srivastava, R., and Koh, J. "Utilization of zeolites as CO_2 capturing agents: Advances and future perspectives", *J. CO_2 Util.*, **41**, p. 101251 (2020).
DOI: 10.1016/j.jcou.2020.101251

26. Guo, Y., Xiang, B., Zhao, B., et al. "Removal of H_2S from simulated blast furnace gas by adsorption over metal-modified 13X zeolite", *Fuel*, **338**, p. 127261 (2023).
DOI: 10.1016/j.fuel.2022.127261

27. Chen, Y., Wang, B., Zhao, L., et al. "New Pebax®/zeolite Y composite membranes for CO_2 capture from flue gas", *J. Memb. Sci.*, **495**, pp. 415–423 (2015).
DOI: 10.1016/j.memsci.2015.08.045

28. Treacy, M.M.J. and Higgins, J.B., *Collection of Simulated XRD Powder Patterns for Zeolites*, 5th Edn., Elsevier, New York, USA (2007).
DOI: 10.1016/B978-0-444-53067-7.X5470-7

29. Karamouz, F., Maghsoudi, H., and Yegani, R. "Synthesis and characterization of high permeable PEBA membranes for CO_2/CH_4 separation", *J. Nat. Gas Sci. Eng.*, **35**, pp. 980–985 (2016). DOI: 10.1016/j.jngse.2016.09.036

30. Elyasi Kojabad, M., Momeni, M., Babaluo, A.A., et al. "PEBA/PSf multilayer composite membranes for CO_2 separation: Influence of dip coating parameters", *Chem. Eng. Technol.*, **43**, pp. 1451–1460 (2020).
DOI: 10.1002/ceat.201900262

31. Medeiros-Costa, I.C., Laroche, C., Pérez-Pellitero, J., et al. "Characterization of hierarchical zeolites: Combining adsorption/intrusion, electron microscopy, diffraction and spectroscopic techniques", *Microporous Mesoporous Mater.*, **287**, pp. 167–176 (2019).
DOI: 10.1016/j.micromeso.2019.05.057

32. Singh, H.K.K., Amin, K., and Arshad, S.E. "Ion exchange capacity of zeolite A with zinc nitrate and its antimicrobial activity", *Pure App. Chem.*, **93**(1),

pp. 39–46 (2021).
DOI: 10.1515/pac-2019-0811

33. Ardestani, M.A., Babaluo, A.A., Peyravi, M., et al. "Fabrication of PEBA/ceramic nanocomposite membranes in gas sweetening", *Desalination*, **250**, pp. 1140–1143 (2010).
DOI: 10.1016/j.desal.2009.09.127

Biographies

Mohammad Javad Vaezi received the BSc degree in Chemical Engineering from Sahand University of Technology, Tabriz, Iran, in 2010, MSc in Chemical Engineering from Sahand University of Technology in 2012, and PhD in Chemical Engineering from Sahand University of Technology in 2018. He is currently an Assistant Professor of Chemical Engineering at Sahand University of Technology. His research interests is in the general area of separation science, the gas separation by membrane process, including hydrogen and natural gas purifications and water purification and treatment by mesoporous zeolite membrane. He has published over 20 research articles on related subjects. In the last years, he presented different courses of chemical engineering which some of them are: Fluid mechanics; Physical chemistry; Thermodynamic. And now he continues his research in Sahand University of technology in the field of mesoporous and microporous Zeolite membrane for natural gas purification and water treatment.

Hasan Bagheri is currently a Professor at Baqiyatallah Medical Sciences University. In addition, He is the Head of Chemical Injuries Research Center at Baqiyatallah Medical Sciences University. His research interests is in the analytical chemistry, electrochemical sensors and biosensors. The research interests of his group at the Chemical Injuries Research Center include: Electrochemical and colorimetric biosensors for screening, diagnostics, and environmental monitoring, electrochemical sensors (Voltammetric and potentiometric), paper-based biosensors, synthesis and characterization of new functionalized nano/micro materials for fabricating of new sensing layers. He has published over 100 research articles on related subjects and now he continues his research in Baqiyatallah Medical Sciences University at professor position.